ACS APPLIED MATERIALS & INTERFACES

Research Article

www.acsami.org

Fast Response and High Sensitivity of ZnO Nanowires—Cobalt Phthalocyanine Heterojunction Based H_2S Sensor

Ashwini Kumar,[†] Soumen Samanta,[†] Ajay Singh,[*,†] Mainak Roy,[‡] Surendra Singh,[§] Saibal Basu,[§] Mohmad M. Chehimi,[∥] Kallol Roy,[⊥] Niranjan Ramgir,[†] M. Navaneethan,[#] Y. Hayakawa,[#] Anil K. Debnath,[†] Dinesh K. Aswal,[*,†] and Shiv K. Gupta[†]

[†]Technical Physics Division, [‡]Chemistry Division, [§]Solid State Physics Division, and [⊥]Research Reactor Maintenance Division, Bhabha Atomic Research Center, Mumbai 400 085, India

[∥]University Paris Diderot, Sorbonne Paris Cité, ITODYS, CNRS, F-75013 Paris, France

[#]Research Institute of Electronics, 3-5-1, Johoku, Shizuoka University, Hamamatsu, Japan

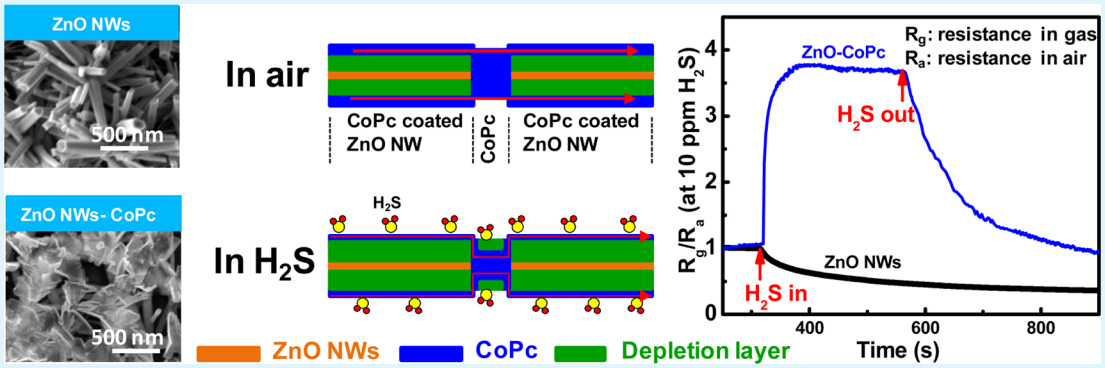

ABSTRACT: The room temperature chemiresistive response of n-type ZnO nanowire (ZnO NWs) films modified with different thicknesses of p-type cobalt phthalocyanine (CoPc) has been studied. With increasing thickness of CoPc (>15 nm), heterojunction films exhibit a transition from n- to p-type conduction due to uniform coating of CoPc on ZnO. The heterojunction films prepared with a 25 nm thick CoPc layer exhibit the highest response (268% at 10 ppm of H_2S) and the fastest response (26 s) among all samples. The X-ray photoelectron spectroscopy and work function measurements reveal that electron transfer takes place from ZnO to CoPc, resulting in formation of a p−n junction with a barrier height of 0.4 eV and a depletion layer width of ∼8.9 nm. The detailed XPS analysis suggests that these heterojunction films with 25 nm thick CoPc exhibit the least content of chemisorbed oxygen, enabling the direct interaction of H_2S with the CoPc molecule, and therefore exhibit the fastest response. The improved response is attributed to the high susceptibility of the p−n junctions to the H_2S gas, which manipulates the depletion layer width and controls the charge transport.

KEYWORDS: *heterojunction, gas sensor, zinc oxide, metal phthalocyanine, depletion layer*

1. INTRODUCTION

Hydrogen sulfide (H_2S) gas is generated in various industrial processes including natural gas processing and petroleum refining. H_2S is a colorless, highly toxic and flammable gas, which is extensively used in many industrial processes.[1,2] H_2S exposure in high concentration can cause damage to the nervous system of the human being.[3] The long and short-term exposure limits for H_2S are 10 ppm for 8 Hrs and 50 ppm for 10 min, which has initiated the research on the development of H_2S sensors that can detect it in the 10−50 ppm range.[2] For H_2S sensor metal oxide semiconductors e.g., SnO_2, CuO, SnO_2/CuO hybrids, WO_3, TiO_2, In_2O_3, ZnO, etc. have been used as the chemiresistive sensing element due to high sensitivity, reasonable stability and ease of operation.[2−33] Owing to their large surface-to-volume ratio nanostructured metal oxide semiconductors such nanowires, nanoparticles, nanobelts, etc., exhibited high sensitivity.[11−15,17−35] However, metal oxides based sensors has limitations in terms of operating and relatively poor selectivity.[2] In order to enhance the selectivity for H_2S, hybrid metal oxides e.g. SnO_2:CuO that form p−n junctions have been employed.[2,16,33,34] These hybrid metal oxides p−n junctions also enhances the sensitivity for H_2S due to large reduction in barrier height.[33−37]

Organic semiconductors, such as metal phthalocyanines (MPcs), porphyrins, pentacene etc have been investigated for gas sensing applications owing to the facile fabrication, operation at room temperature and low fabrication cost.[38−49] In MPcs charge carriers can be generated/depleted on

Received: April 29, 2015
Accepted: July 30, 2015
Published: July 30, 2015

DOI: 10.1021/acsami.5b03652
ACS Appl. Mater. Interfaces 2015, 7, 17713−17724

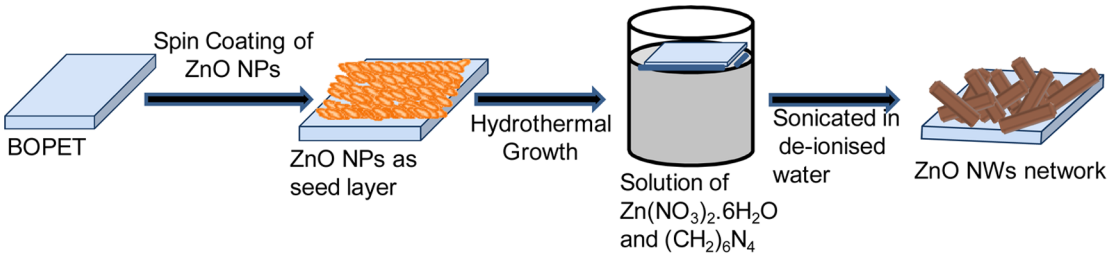

Figure 1. Steps involved in the synthesis of ZnO nanowire films on BOPET substrates.

Figure 2. Schematic showing the modification of a ZnO nanowire network by CoPc.

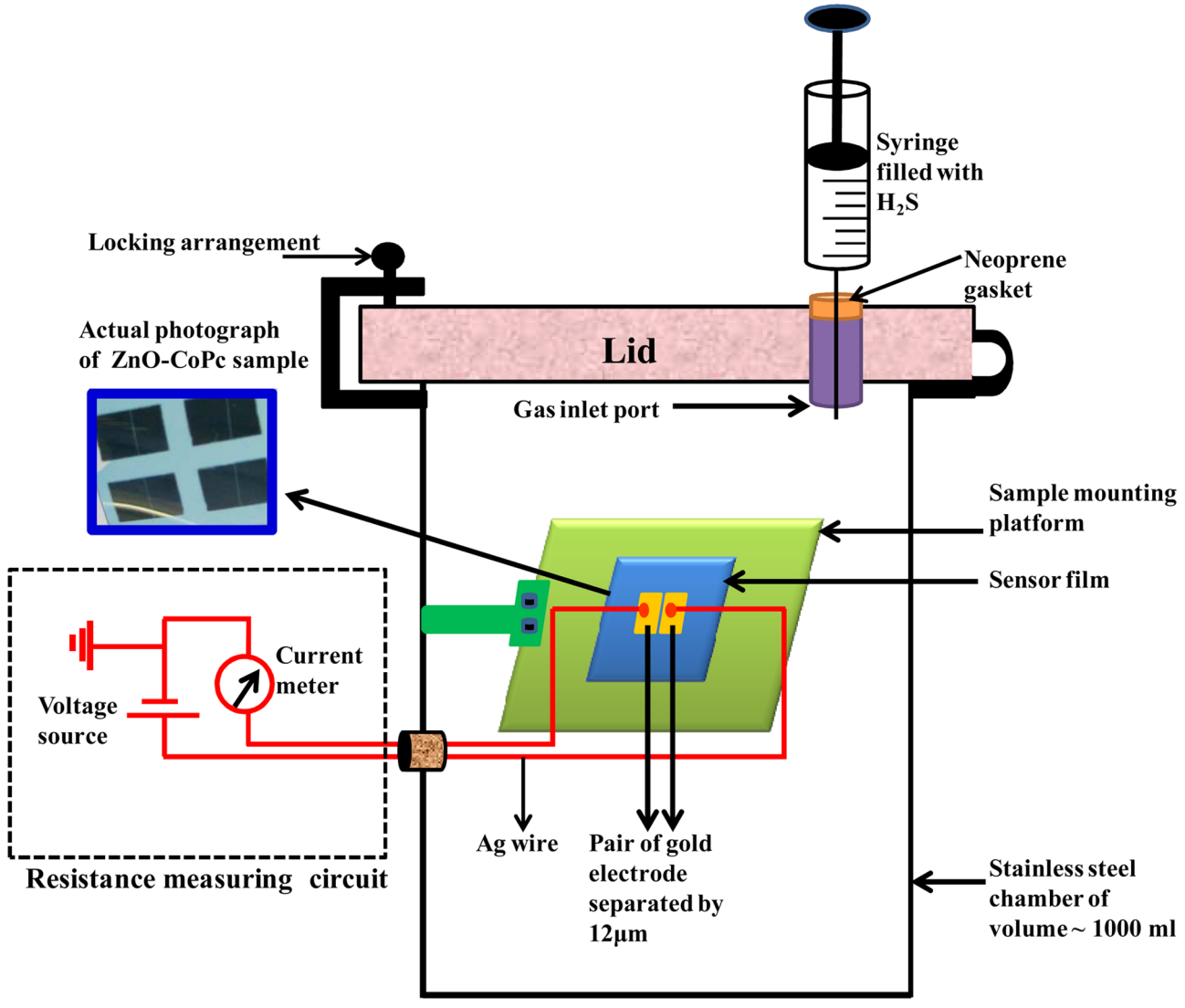

Figure 3. Schematic of the gas sensing set up and electrical measurement unit. The actual photograph of a ZnO-CoPc (25 nm) sample having 4 pairs of gold electrodes (separated by a 12 μm gap) is also shown here.

DOI: 10.1021/acsami.5b03652
ACS Appl. Mater. Interfaces 2015, 7, 17713−17724

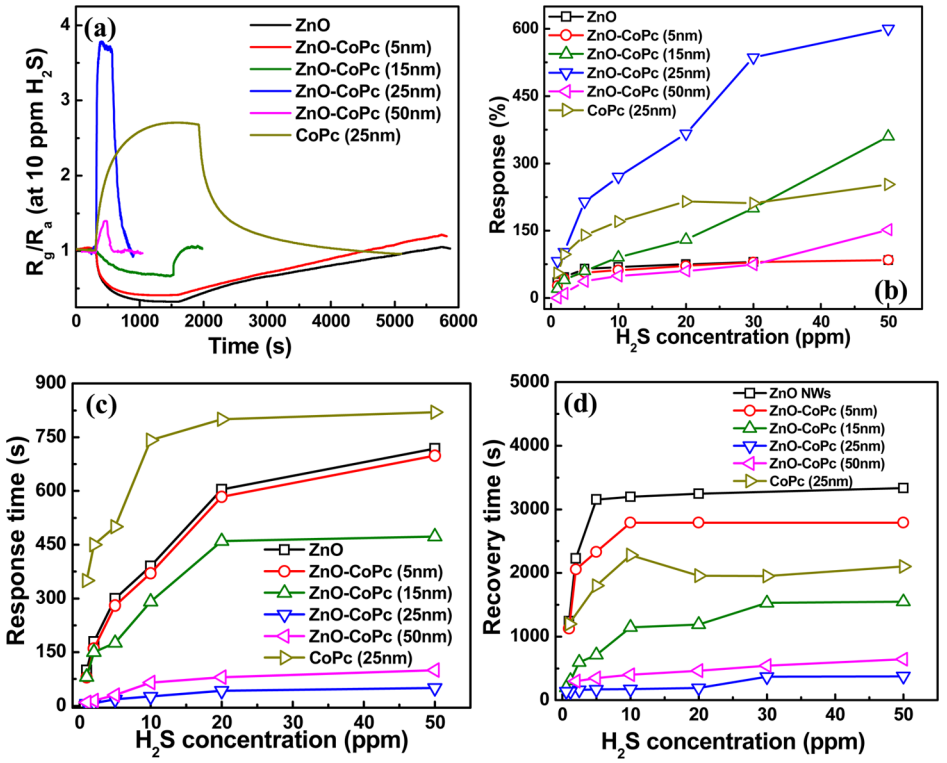

Figure 4. (a) Typical response curve (i.e., normalized resistance versus time) of all samples on 10 ppm exposure of H_2S gas. Here R_g and R_a stand for resistance in the presence of gas and air, respectively. (b) Response (%) as a function of H_2S concentration. (c) Response time. (d) Recovery time as a function of H_2S concentration.

interaction with analyte through the redox process. However, MPc due to room temperature operation results in higher response and recovery times.[41,42,45] In addition they also lack in the specificity. In order to lower the response/recovery times and improve selectivity the hybrid materials comprising of organic−inorganic semiconductors has been employed.[35,46,47] For example metal oxide/conducting polymer based on ZnO-poly(3-hexylthiophene) and ZnO-polypyrrole, exhibit enhanced selectivity but their sensitivity and response kinetics remains unaffected.[35,46] On the other hand metal oxide/molecular semiconductor such as ZnO-metal phthalocyanine have not been employed yet for the gas sensing application. It may be noted that such metal oxide/metal phthalocyanine based composite structures are widely being explored for interface study, solar cell, diode applications.[50−53] In this paper, we demonstrate that the modification of a network of ZnO nanowires with cobalt phthalocyanine thin films not only improves the sensitivity for H_2S but also lowers down the response time drastically.

2. EXPERIMENTAL SECTION

2.1. Growth of ZnO Nanowires Films on BOPET Sheet. A random network of ZnO nanowires (ZnO NWs) was grown on biaxially oriented polyethylene terephathalate (BOPET) flexible substrate by hydrothermal method using presynthesized ZnO nanoparticles as seed.[36,54] Figure 1 schematically shows the different steps involved in the fabrication process. First ZnO nanoparticles (NPs) were prepared by dissolving Zinc acetate dihydrate (0.015M) in methanol (100 mL) under strong stirring at 60 °C. Later a 0.03 M solution of sodium hydrooxide in methanol (50 mL) was added slowly at 60 °C.[36] The volume ratio of two solutions was maintained as 2:1. The reaction mixture was stirred for 2 h at 60 °C. The resulting nanoparticles in solution were having diameter between 5 and 10 nm and were stable for a period of around 2 weeks.[36] Coating of ZnO nanoparticles on BOPET substrates was done by spin coating of as synthesized nanoparticle solution. The growth of ZnO NWs on these coated BOPET sheets was carried out by suspending these sheets over a solution containing aqueous equimolar (25 mM) concentration of Zinc nitrate and Hexamethylenetetramine (HMTA), $(CH_2)_6N_4$ at 90 °C for approximately 7 h.[36] After growth the substrates were thoroughly washed with deionized water and dried under Ar flow. The growth of ZnO NWs on BOPET substrate was found to be very reproducible for the same condition of temperature and solution concentrations. In the present work, BOPET was chosen as substrate due to the presence of polar ester groups in the PET chains. Since ZnO also has polar surfaces therefore ZnO NWs grown on BOPET exhibit a good adhesion with the substrate due to dipolar attraction.[41] In addition the BOPET substrate has added advantage of flexibility, lightweight and low cost.

2.2. Modification of ZnO Nanowires Films by Cobalt Phthalocyanine. The network of ZnO NWs films deposited on BOPET sheet was modified with different thicknesses (viz.; 5 nm, 15 nm, 25 and 50 nm) of CoPc as shown schematically in Figure 2. The CoPc thin films were synthesized using conventional thermal evaporation at high vacuum (~2.5×10^{-6} mbar) condition. During deposition of CoPc layer, ZnO NWs coated BOPET substrate was maintained at room temperature. The thickness of films was monitored in situ through a quartz crystal monitor. Hereafter these samples will be referred as ZnO-CoPc (d nm), where d is the nominal thickness of the CoPc layer.

2.3. Characterization. The structural characterization of the samples was carried out by X-ray diffraction (XRD) (model: Bruker D8 Focus diffractometer). The samples were characterized by scanning electron microscopy (SEM) (Model: Vega, MV 2300/T40, Tescan). Raman spectroscopy of the samples was carried out using He-Neon laser ($\lambda \sim 632.81$ nm) as excitation source. The X-ray photoelectron spectroscopy (XPS) of samples was carried out using Mg K_α (1253.6 eV) radiation and the recorded data was calibrated using C-1s peak from the adventitious carbon-based contaminant with the binding energy of 284.6 eV. The electronic absorption spectra were recorded

DOI: 10.1021/acsami.5b03652
ACS Appl. Mater. Interfaces 2015, 7, 17713−17724

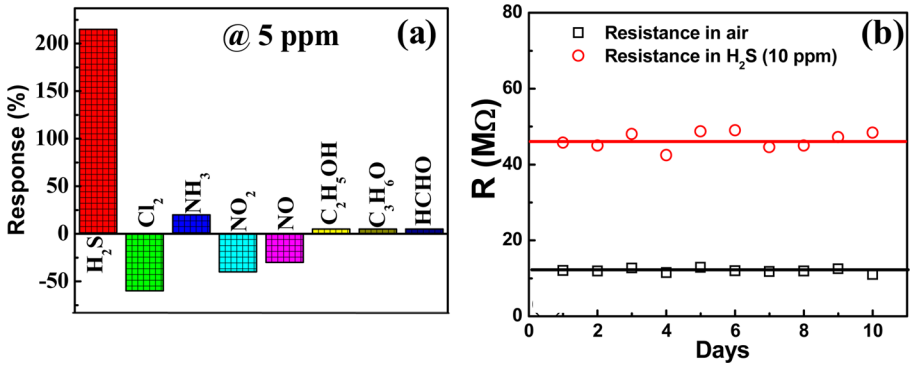

Figure 5. (a) Selectivity histogram (measured at 5 ppm) of ZnO-CoPc (25 nm) samples for different gases. (b) Stability measurement of ZnO-CoPc (25 nm) sample performed over a period of 10 upon repeated exposure to 10 ppm of H_2S.

using UV−vis spectrophotometer (JASCO, Japan). Photoluminescence (PL) measurements were done at room temperature on an Edinburgh Instruments FLSP 920 system. For PL experiments xenon lamp (450W) and a microsecond flash lamp (60 W) were used for excitation and a photomultiplier tube was used as the detector. In order to measure the electrical resistance of the films, electrical contacts were prepared by first thermally depositing two gold pads (80 nm thick, size 2 mm × 2 mm at a spacing of 12 μm) onto films and then attaching silver wires (diameter ∼100 μm) to the films by silver paint. The chemiresistive gas sensing characteristics i.e. the resistance (R) versus time (t) data for the samples was recorded on exposure to different oxidizing and reducing gases (i.e., H_2S, NH_3, NO_2, NO, Cl_2, C_2H_5OH etc.) in a static gas sensing unit of volume ∼1000 mL, which is schematically shown in Figure 3. For gas sensing experiment the films were mounted on a platform in a leak tight stainless steel chamber (net volume: 1000 mL). A desired concentration of the test gas in the chamber was achieved by injecting a known quantity of gas using a microsyringe.

The resistance of the samples was measured through an electrical circuit (shown in Figure 3) that consists of a voltage source and current ammeter system. The response data was acquired by a personal computer equipped with Labview software. At a particular gas exposure, once the response of sensor film is saturated (constant resistance with respect to time), recovery of sensors was recorded by exposing the sensors to air by opening the lid of the chamber. From the response data of the sensor, response (%) is calculated using the relation:[2]

$$S\% = \left|\frac{Rg - Ra}{Ra}\right| \times 100 \quad (1)$$

where R_a and R_g are the values of resistance in air and H_2S gas, respectively.

Response and recovery times for the sensor were defined as the time needed for 90% of total resistance change on exposure to H_2S gas and air, respectively.

3. RESULTS AND DISCUSSION

Typical normalized response curves of pure ZnO NWs films and ZnO NWs - CoPc (having different thickness) films for 10 ppm of H_2S are shown in Figure 4(a). From Figure 4(a) following inferences can be drawn: (i) Pure ZnO NW films and heterojunction films with CoPc thickness ≤15 nm exhibit a decrease in resistance on H_2S exposure indicating the n-type conduction. (ii) Pure CoPc films of thickness ∼25 nm exhibit an increase of resistance when exposed to H_2S, suggesting a p-type conduction. (iii) Heterojunction films with CoPc thickness of ∼25 nm exhibit a huge increase in the resistance on exposure to H_2S indicating that now CoPc starts playing a dominant role in conduction; hence a p-type behavior is observed. (iv) With further increase of CoPc thickness (>25 nm) the response and recovery of heterojunction films becomes sluggish.

The response (%) data for all samples is plotted in Figure 4(b). It can be seen that heterojunction films with CoPc thickness of ∼25 nm exhibit highest response (%) in comparison to all other samples. The response time and recovery time data for all samples are shown respectively in Figure 4(c) and Figure 4(d). From there it can be seen that ZnO-CoPc (25 nm) sample exhibit the fastest response and recovery (response time ∼26 s and recovery time ∼175 s at 10 ppm of H_2S) among all samples. It is also important to note that pure ZnO and pure CoPc films exhibit slow response kinetics.

Selectivity histogram for the ZnO-CoPc (25 nm) films is shown in Figure 5(a), which shows that these films are highly selective to the H_2S gas. Moreover, these heterojunction films were stable in atmospheric conditions for several months. Figure 5(b) shows the stability measurement of ZnO-CoPc (25 nm) films performed over a period of 10 days, the obtained result suggests that these films are quite stable (variation of about 10%) even after repeated exposure to 10 ppm of H_2S. The enhanced response (%), selectivity, fast response/recovery and stability at repeated exposure qualify these heterojunction films for rapid detection of H_2S in the range of 1−50 ppm at room temperature.

In the following we investigate why among all samples why ZnO-CoPc (25 nm) films exhibit highest response (%) and fastest response for the H_2S gas. In Figure 6(a) we have shown the schematic as well as SEM images of all samples. From Figure 6(b) it can be seen that pure ZnO NWs films makes a porous network of NWs and the typical diameter of these NWs is in the range of 50−110 nm and length in the range of 1−2 μm. The quasi-hexagonal ends of the ZnO NWs indicate that their main axis is preferentially oriented along [0001] direction, which is in accordance with the growth tendency of wurzite crystals.[36] The surface morphology of the ZnO NWs films did not change upon deposition of CoPc layer up to a nominal thickness of 5 nm and this is expected as at low thickness of CoPc it tries to cover the surface of ZnO NWs. Since in the response data shown in Figure 4(a), where ZnO−CoPc (5 nm) films exhibit n-type behavior, which suggest that at low thickness of CoPc does not uniformly cover the surface of ZnO NWs and as a result n-type conduction of the ZnO NWs dominates the response. The morphology of the ZnO-CoPc (15 nm) films exhibit slight increase in the diameter of the ZnO NWs (shown in Figure 6(c)) suggesting the increasing coverage of CoPc on ZnO-NWs surface. From SEM image

DOI: 10.1021/acsami.5b03652
ACS Appl. Mater. Interfaces 2015, 7, 17713−17724

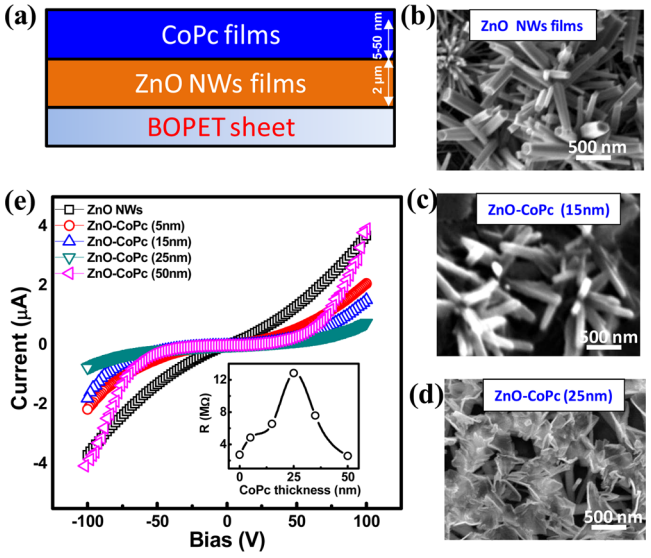

Figure 6. (a) Schematic of the hybrid films on the BOPET sheet. (b–d) SEM images of the pure ZnO and hybrid films. (d) In-plane current–voltage characteristics of all samples. Inset shows the resistance of the hybrid films as a function of CoPc thickness.

shown in Figure 6(d), it can also be seen that the increase of CoPc thickness up to 25 nm, the ZnO NWs gets uniformly coated and in addition there is also a formation of thin lamellar sheets of CoPc interconnecting the CoPc coated ZnO NWs. The p-type conduction of ZnO NWs – CoPc (25 nm) sample also suggest that in these samples the ZnO NWs are uniformly coated with the CoPc.

Figure 6(e) shows the typical in-plane current–voltage characteristics of all samples in the bias range of ±100 V. One of the intriguing observations in the Figure 6(e) is that heterojunction films with increasing CoPc thickness up to 25 nm exhibit lowering of current (at a fixed bias), while for higher CoPc thickness current enhances and reaches nearly close to the pure ZnO NWs films. To see this clearly, in the inset of Figure 6(e), the base resistance (measured at 100 V) of all sample is plotted. From inset of Figure 6(e) it can be seen that heterojunction films with CoPc thickness ∼25 nm exhibit highest resistance among all samples and we later provide the explanation for this behavior. It is also interesting to note that ZnO NWs-CoPc (50 nm) sample exhibit a typical *I*–*V* characteristics which is similar to pure CoPc films, where with increasing bias (>10 V) an ohmic to space charge limited conduction takes place.[40]

The transmission microscope (TEM) images of the pure ZnO and ZnO-CoPc (25 nm) heterojunction films are shown in Figure 7. As seen from Figure 7(a), the average diameter of the pure ZnO nanowires is around ∼110 nm. The high resolution TEM image shown in inset of Figure 7(a) reveals that these ZnO wire are polycrystalline in nature. From the TEM images shown in Figure 7(b) it can be seen that the estimated thickness of CoPc overlayer on ZnO nanowires in heterojunction films is close to the nominal thickness obtained from quartz crystal monitor. The TEM image shown in Figure 7(b) also reveals that CoPc layer grown on CoPc are not highly ordered.

The typical Co $2p_{3/2}$, and Zn $2p_{3/2}$ XPS spectra of all samples are shown respectively in Figure 8 (a) and 8(b). The respective binding energy value for Co $2p_{3/2}$ (in pure CoPc film) and Zn $2p_{3/2}$ (in pure ZnO NWs films) were found to be 781.8 and

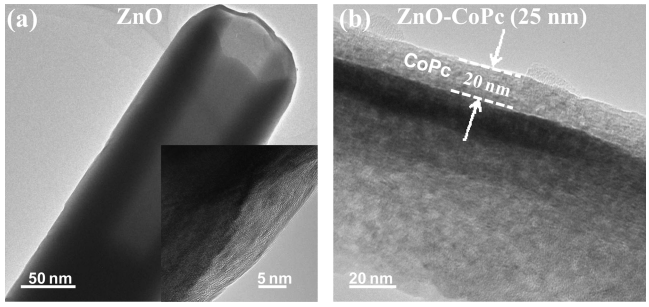

Figure 7. TEM images of the (a) pure ZnO nanowire; inset showing the high resolution image of ZnO. (b) ZnO-CoPc (25 nm) heterojunction films.

1020.6 eV.[42,43,55] From Figure 8(a) it is evident that in comparison to pure CoPc films, the heterojunction films exhibits a shift of Co $2p_{3/2}$ peak toward lower binding energy with increasing CoPc thickness. On the other hand for heterojunction samples, with increasing CoPc thickness, Zn $2p_{3/2}$ peak exhibit a shift toward higher binding energy in comparison to the pure ZnO NWs films. Such a shift of XPS peaks indicates the electron transfer from ZnO NWs to CoPc. Since adsorbed oxygen plays a very important role in the gas sensing behavior of ZnO and CoPc films therefore for heterojunction films we have measured the ratio of chemisorbed oxygen to the Co and result is plotted in Figure 8(c). It can be seen that for ZnO-CoPc (25 nm) sample exhibits the least content of chemisorbed oxygen. It may be noted that in heterojunction with increasing thickness of CoPc the XPS signal from ZnO NWs become weak in intensity. From the XPS data, we have estimated the actual thickness of CoPc layer grown on ZnO NWs surface, which was determined from the attenuation of the intensities of characteristic Zn $2p_{3/2}$ and Zn $2p_{1/2}$ peaks.[56]

According to Beer–Lambert law, the peak intensities (peak area) are expressed by[56]

$$I_{2p_{3/2}} = I^0_{2p_{3/2}} e^{-d/\lambda_{2p_{3/2}}\sin\theta} \quad (2)$$

and

$$I_{2p_{1/2}} = I^0_{2p_{1/2}} e^{-d/\lambda_{2p_{1/2}}\sin\theta} \quad (3)$$

Where *I* is the peak intensity of the core level electron $2p_{3/2}$ or $2p_{1/2}$ recorded for CoPc coated ZnO NWs, while I° corresponds to the peak intensity obtained from bare ZnO NWs. Zn $2p_{3/2}$ and Zn $2p_{1/2}$ intensity ratios can be calculated for bare and coated ZnO NWs:

$$R^0 = I^0_{2p_{3/2}}/I^0_{2p_{1/2}} \quad (4)$$

and

$$R = I_{2p_{3/2}}/I_{2p_{1/2}} \quad (5)$$

Combining eqs 2-5 leads to the analytical expression for assessing the thickness:

$$d = \sin\theta/[(\lambda_{2p_{3/2}})^{-1} - (\lambda_{2p_{1/2}})^{-1}]\ln(R_0/R) \quad (6)$$

The analyses were performed at an emission angle of 90°, so sin θ = 1. The attenuation lengths were estimated using the Seah and Dench equation established for an organic coating:

$$\lambda = 0.11(E_k^{1/2}) \text{ in mg/m}^2 \quad (7)$$

DOI: 10.1021/acsami.5b03652
ACS Appl. Mater. Interfaces 2015, 7, 17713–17724

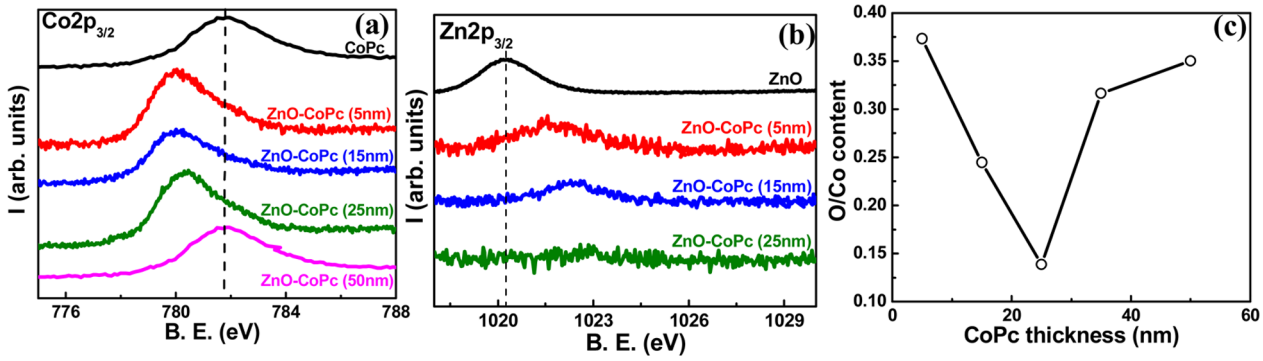

Figure 8. XPS spectra of (a) $Co2p_{3/2}$ and (b) $Zn2p_{3/2}$ for the ZnO NWs and heterojunction films. (c) O/Co content for ZnO-CoPc heterojunction films.

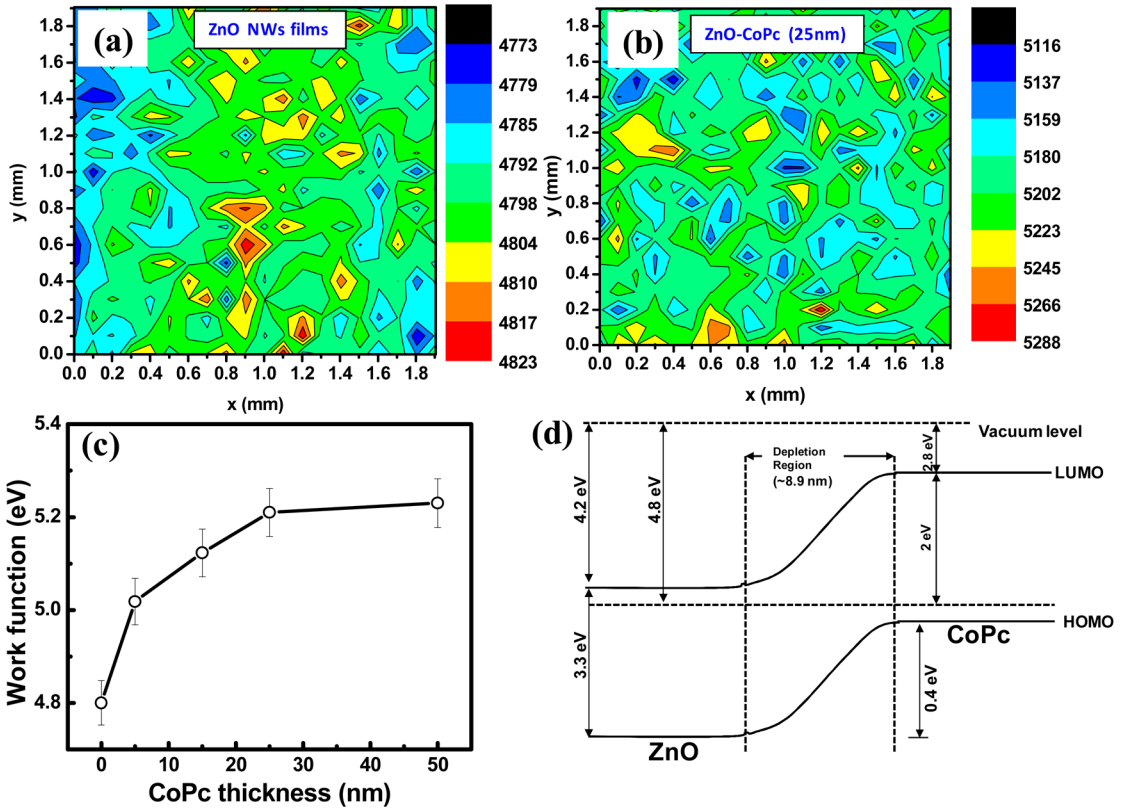

Figure 9. Work function mapping (scan area: 2 mm × 2 mm) of (a) ZnO NWs and (b) ZnO-CoPc (25 nm) samples. (c) Plot showing the work function of hybrid films as a function of CoPc thickness. (d) Schematic of the energy level alignment at the ZnO−CoPc interface.

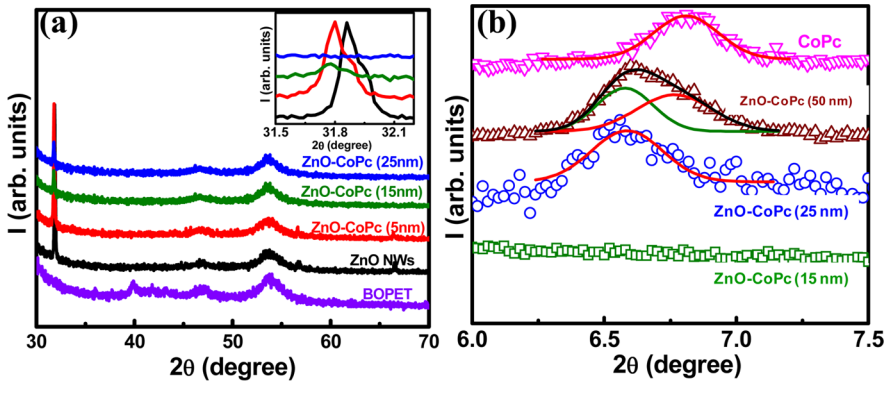

Figure 10. (a) XRD data and (b) GIXRD data for the pure ZnO NWs, pure CoPc, and ZnO−CoPc heterojunction films.

DOI: 10.1021/acsami.5b03652
ACS Appl. Mater. Interfaces 2015, 7, 17713−17724

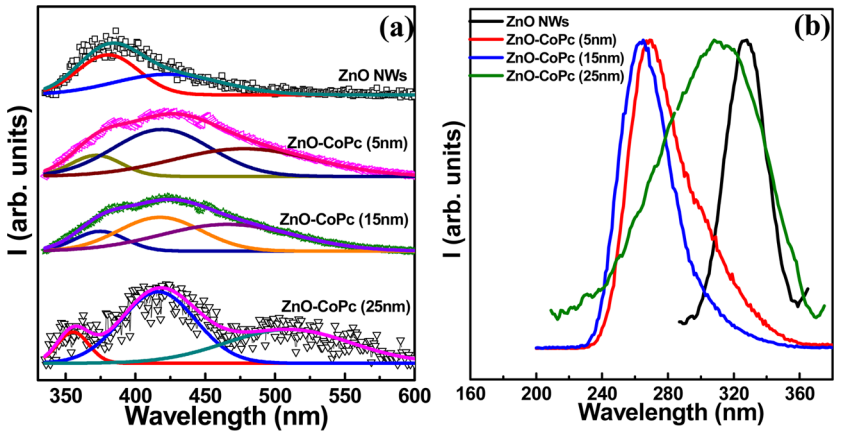

Figure 11. Photoluminescence (a) emission and (b) excitation spectra for all samples.

where E_K is the kinetic energy of the core level electron Zn $2p_{3/2}$ (~232 eV) or Zn $2p_{1/2}$ (~210 eV). It follows that for determining the thickness (in nm), one has to divide λ in mg/m^2 by the overlayer density in g/cm^3 which is taken as ~1.6 for CoPc layer. eq 7 permits to estimate the attenuation length to 1.59 and 1.68 nm for Zn $2p_{3/2}$ and Zn $2p_{1/2}$, respectively. Applying these values in eq 6 yields a CoPc layer thickness of 22.2 nm which is quite close to the nominal CoPc thickness of ~25 nm.

The possibility of charge transfer between ZnO and CoPc is further supported by the work function measurement. The typical work functions mapping results for ZnO NWs and ZnO-CoPc (15 nm) films are shown in Figure 9(a) and 9(b) respectively. As seen from Figure 9(c), for pure ZnO NWs films the work function was found to be 4.8 eV and for heterojunction films it systematically increases with increasing CoPc thickness and attains a value 5.2 eV (i.e., comparable to the pure CoPc) at nominal thickness of 25 nm. The difference in work function of ZnO NWs and CoPc suggest that at the interface there is a transfer of charge from ZnO to CoPc resulting in the formation of a p−n junction with effective barrier height of 0.4 eV (shown schematically in Figure 9(d)).

The XRD data for all samples are shown in Figure 10. In the X-ray diffraction data (shown in Figure 10(a)) obtained in the range of 30−70° we observe diffraction peaks at 2θ = 31.5°, 56.5° and 66.3°, which are attributed to diffraction from the (100), (110) and (200) atomic planes of hexagonal wurtzite phase of ZnO. The estimated lattice parameters of the ZnO was found to be a = 3.2480 Å and c = 5.2068 Å with c/a= 1.6031 and cell volume= 47.57 Å^3. The obtained lattice parameters are consistent with the reported literature values.[57] Inset of Figure 10(a) shows the XRD patterns (enlarged view of only 31.5° diffraction peak corresponding to the (100) reflection of ZnO) of all samples. Large broadening of diffraction peak suggests the nanocrystalline nature of the ZnO. For heterojunction films with increasing thickness of CoPc layer there are following two important points are noticed from XRD data shown in inset of Figure 10(a): (i) (100) diffraction peak of ZnO NWs systematically shifts to the lower 2θ values and (ii) (100) diffraction peak exhibit lowering of intensity as well as broadening. Both of these observations suggest that interaction between CoPc and ZnO NWs creates structural defects in the ZnO NWs close to the ZnO-CoPc interface.

It is important to mention that CoPc diffraction peak usually observed at low diffraction angles (<10°) due to its large lattice parameters, therefore to obtain the information about the crystalline nature of CoPc in heterojunction films, the diffraction data was collected in the grazing incidence mode. In the grazing incidence X-ray diffraction data (GIXRD) shown in Figure 9(b), the (200) diffraction peak corresponding to CoPc layer is observed at low angles. From Figure 10(b) it can be seen that in the heterojunction films with CoPc thickness ≤15 nm the CoPc does not exhibit crystalline nature (i.e., absence of diffraction peak). For ZnO-CoPc (25 nm) sample the diffraction peak corresponding to CoPc is observed at ~6.52°. However, for ZnO-CoPc (50 nm) sample the CoPc diffraction peak become asymmetric toward higher diffraction angle and it can be deconvoluted into two peaks, one at 6.52° corresponding to CoPc in immediate vicinity of ZnO NWs and other at 6.8° (i.e., exactly at same position for pure CoPc films) corresponding to the relaxed CoPc layer which is far from ZnO surface.[58] In summary, the XRD data suggest, CoPc layer in close proximity to ZnO -CoPc interface initially grows in a disordered way but later (i.e., around CoPc thickness of ~25 nm) at full coverage it attains a crystalline nature. The XRD data also suggest that the interaction of CoPc with ZnO NWs affects the molecular ordering of CoPc layer near the interface. As discussed earlier, there is a charge transfer from ZnO NWs to the CoPc molecules, which may affect the planarity of the CoPc molecule as a result the interplanar distance between the CoPc molecules increases and it shifts the diffraction peak of heterojunction films (with 25 nm thick CoPc) to lower angles.

Figure 11(a) shows the photoluminescence (PL) emission spectra of all samples. When pure ZnO NWs sample is excited with light of wavelength ~320 nm, it shows an emission line at ~380 nm, which is assigned to the near band edge (NBE) transition and an asymmetric band trailing at higher wavelength region (peak around 420 nm) due to defect originated from the oxygen vacancies.[36] From the PL emission spectra of heterojunction films following inferences can be drawn: (i) The NBE peak exhibit a blue shift with increasing thickness of CoPc. For ZnO -CoPc (25 nm) sample the NBE peak is observed at ~355 nm (ii) In addition to the defect related emission peak at ~420 nm, heterojunction films initially at low thickness of CoPc exhibit an additional peak at ~480 nm and it shift to 510 nm for the ZnO -CoPc (25 nm) sample. By taking the area ratio of defect related emission (combining the contributions of 420 nm peak and other higher wavelength peak) to band edge emission, we could estimate the contribution of defect related emission as ~47% for pure

DOI: 10.1021/acsami.5b03652
ACS Appl. Mater. Interfaces 2015, 7, 17713−17724

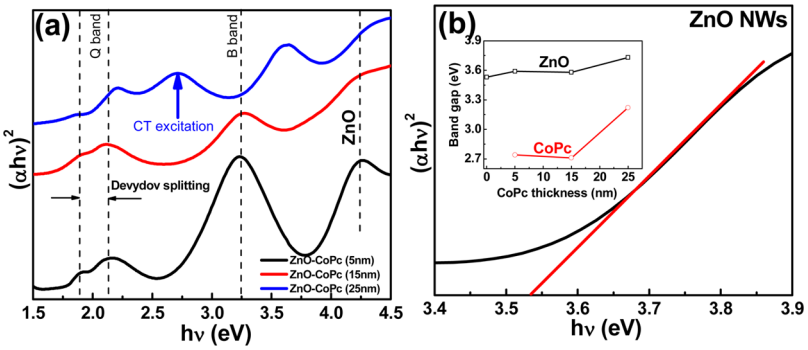

Figure 12. Electronic absorption spectra recorded for (a) pure ZnO NWs films and (b) for heterojunction films; here, the *y*-axis is plotted on log scale. Inset of part a shows the estimated band gap value for ZnO and CoPc in the heterojunction films.

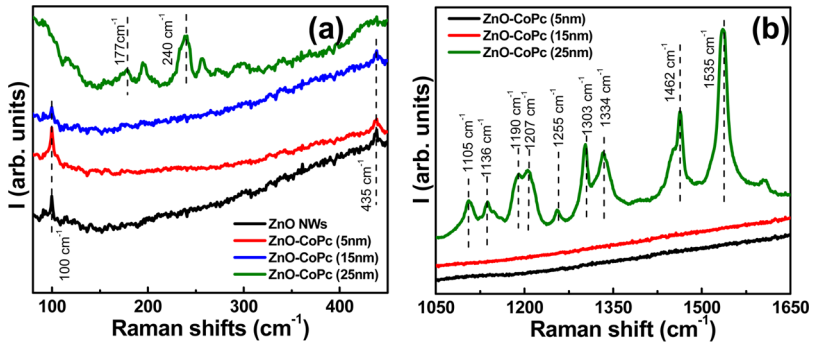

Figure 13. Raman spectra for all samples: (a) low wavenumber region 80−450 cm^{-1}; (b) high wavenumber region 1050−1650 cm^{-1}.

ZnO NWs sample while for heterojunction films it increases with the thickness of CoPc layer. For ZnO - CoPc (25 nm) sample the contribution of defect related emission is found to be nearly 88%. The suppression of band edge emission in heterojunction films can be explained by the formation of p−n junction between p-type CoPc and n-type ZnO NWs. When a photon is incident on the films an exciton is formed. The p−n junction enhances the dissociation of exciton due to built in field. The electrons which is released by dissociation of exciton is taken away by the ZnO layer and CoPc layer transports the holes. Hence the dissociation of excitons suppresses the electron−hole recombination which is necessary for PL band edge emission. The extent of interaction between ZnO NWs and CoPc is also manifested in the excitation profile of the samples (shown in Figure 11(b)). The excitation spectra of heterojunction films exhibit blue shift and broadening with respect to the pure ZnO NWs sample. For ZnO−CoPc (25 nm) sample the excitation spectra exhibit very large broadening, which extends from 220 to 360 nm and it suggest that in case the conduction band of ZnO is highly perturbed by the presence of CoPc layer.

Figure 12(a) shows the electronic absorption spectra for pure ZnO NWs and heterojunction films. The estimated bang gap for pure ZnO NWs is found to be 3.6 eV.[35,50] Some interesting features has been observed in the electronic absorption spectra of CoPc in the heterojunction films. For CoPc films the absorption in the visible region (close to 1.9 eV) is referred as Q-band arising from the singlet $\pi-\pi^*$ transition in the porphyrins ring (i.e., intermolecular excitation) and has a doublet due to Davydov splitting.[59] The difference in the relative orientation of the molecules decides the extent of Davydov splitting. From Figure 12(a) it is evident that magnitude of Davydov splitting remains same at low thickness of CoPc but at higher thickness (~25 nm) of CoPc it enhances, which is consistent with the fact that at low thickness CoPc grows randomly on ZnO but at higher thickness it attains a crystalline nature. For CoPc, the peak in absorption spectra in the near UV region is known as B- band or Sorret band. It is very important to note that for ZnO-CoPc (25 nm) sample we observe a peak at 2.7 eV, the origin of which is attributed to the charge transfer (CT) excitation that is an intermolecular excitation.[59] The energy band gap has been obtained from the electronic absorption spectra using relation:

$$\alpha = \alpha_0(h\nu - E_g)^{1/2} \tag{8}$$

where α is the absorption coefficient, α_0 is a constant and $h\nu$ is the photon energy.

As seen from Figure 12(b), the value of direct band gap E_g estimated for ZnO in pure films was found to be 3.5 eV and for heterojunction films it enhances with increasing CoPc thickness. The band gap of ZnO in the ZnO-CoPc (25 nm) is found to be 3.7 eV, such an enhancement of band gap is attributed to the electronic interaction between ZnO NWs and CoPc layers. For heterojunction film, the increase in E_g of ZnO with increasing CoPc thickness is also supported by the blue shift of NBE peak in the PL emission spectra. For CoPc layer the E_g value estimated from B band is found to be 2.7 eV (at low thickness of CoPc) and it increases to 3.2 eV when CoPc layer thickness is increased to 25 nm. The enhancement of E_g for both ZnO and CoPc layer in the heterojunction ZnO-CoPc (25 nm) films suggest strong electronic interaction between both.

Figure 13(a) and 13(b) respectively shows the Raman spectra in two different wavenumber regions of ZnO-CoPc heterojunction films. The ZnO lattice existing in Wurtzite structure has P63mc symmetry and contains two formula units in each primitive cell.[60] According to the group theoretical

DOI: 10.1021/acsami.5b03652
ACS Appl. Mater. Interfaces 2015, 7, 17713−17724

analysis, the irreducible representation for optical phonons is given by $A_1 + 2B_1 + E_1 + 2E_2$, of which the nonpolar E_2 modes at ~100 cm^{-1} and ~435 cm^{-1} respectively due to the vibrational motion of the Zn sublattice and oxygen atoms forms the two most prominent features in the Raman spectra of our samples.[61] As seen from Figure 13(b), up to 15 nm thickness of CoPc, no Raman peaks that could be assigned to the CoPc layer were observed. Interestingly, the E_2 modes of ZnO gradually increased in intensity with the increasing thickness of the CoPc layer until it completely covered the underlying ZnO layer. As discussed above, XPS data analysis of the heterojunction films suggests that ZnO which is inherently n-type semiconductor due to oxygen vacancies donates electron to the antibonding orbital of the CoPc layer and forms a charge transfer complex. Such electronic interaction complemented by the strain induced structural changes due to lattice mismatch result in the significant change of geometry of vibrational modes and hence the internal reorganization energy. Similar effects have been observed for photoinduced electron transfer in donor−acceptor (D-A) complexes.[62] Such geometric change in the D−A complex may even affect the Raman cross-section and hence the Raman intensities of a few selective bands, as observed in case of the ZnO-CoPc heterojunction films

The intense peaks observed at higher wavenumber region (shown in Figure 13(b)) for ZnO-CoPc (25 nm) and ZnO-CoPc (50 nm) samples are assigned to the different modes of the CoPc molecule signifying the presence of the CoPc overlayer. For these hybrid films, the sharp intense peak at ~1535 cm^{-1} and ~1334 cm^{-1} are respectively assigned to the totally symmetric stretching vibration at the C_β-C_β and C_α-C_β bonds of the pyrrole rings whereas the peak at ~1136 cm^{-1} results from the breathing vibration of the pyrrole rings. These vibrations have been primarily assigned as isoindole ring stretches with large C−N contribution. The Co−N vibration is observed at 240 cm^{-1}. The vibration due to in-phase motion of isoindole group is observed at 177 cm^{-1}.[61] The other peaks assigned at Figure 13(b) matches very well with the reported values for Raman peak of CoPc.[63,64]

Based on charge transport, SEM, XRD, XPS, work function, Raman spectroscopy and PL results, we conclude that in heterojunction films there is a strong interaction between ZnO NW and CoPc layer and sample with CoPc layer thickness ≥25 nm uniformly cover the ZnO NWs. The structure of ZnO NWs consists of tetrahedrally coordinated O^{2-} and Zn^{2+} ions planes which are placed alternately along the *c*-axis. It results in Zn^{2+}-terminated (0001) and O^{2-} terminated $(000\bar{1})$ end polar surfaces results in a normal dipole moment and spontaneous polarization along the *c*-axis of ZnO NWs.[57] In general on polar surfaces at low thickness the CoPc molecules can stacks in a face on manner due to enhanced molecule−substrate interaction, however with increasing thickness molecule−molecule interaction dominates and as a result molecules prefers to stack in edge on manner. Such a competition of face on and edge in stacking pattern of CoPc molecule on polar ZnO surface may leads to the initial growth of CoPc in an amorphous way.

In ZnO-CoPc (25 nm) films in which ZnO NWs are uniformly coated with CoPc (thickness ~25 nm), and transfer of electrons from ZnO NWs to CoPc will reduce the hole concentration in CoPc up to the depletion layer width. The depletion layer width (W) of the p−n junction formed at the ZnO-CoPc interface can be calculated using the following relation:[65]

$$W = \left[\frac{2\varepsilon_{CoPc}V_0}{eN_a} + \frac{2\varepsilon_{ZnO}V_0}{eN_d}\right]^{1/2} \quad (9)$$

Here ε_{CoPc} is the permittivity of the CoPc and it is taken as 3, ε_{ZnO} is the permittivity of the ZnO and it is taken as 8.7, V_0 is the energy barrier (0.4 eV) at ZnO-CoPc interface, e is the electronic charge and N_a is the acceptors concentration at CoPc (equivalent to the hole concentration ~3×10^{16} m^{-3}) and N_d is the donor concentration at ZnO (equivalent to the electron concentration ~1.3×10^{23} m^{-3}). The calculated value of W is ~8.9 nm and since $N_d \gg N_a$ therefore depletion region is mostly extended in the CoPc region around the p-n interface. Since in the present case the ZnO-CoPc (25 nm) sample exhibit least content of chemisorbed oxygen therefore such sample may have very low hole concentration and therefore actual W could be much larger than the estimated value. Since the depletion region obstructs the movement of charges therefore in such heterojunction films the conduction channel is quite narrow and hence these sample exhibit the highest resistance value (as discussed before in Figure 6(e)). At present it is not clear why ZnO-CoPc (25 nm) exhibit the low content of chemisorbed oxygen, possibly it could be the presence of the built in field of the formed p−n junction (which is directed from ZnO NWs to the CoPc side) which may provide the extra barrier for the chemisorptions of oxygen. In hybrid films with thicker CoPc layer (~50 nm) the role of depletion region in obstructing the charge transport will be negligible due to high hole concentration at the surface (due to more chemisorbed oxygen).

Now we present plausible sensing mechanism of detection H_2S i.e. a highly reducing (electron-donor gas). (i) Since ZnO NWs exhibit n-type conduction and when it is exposed to atmosphere, oxygen molecules adsorb on the surface of the ZnO NWs and form O_2^- ions by capturing electrons. Thus, ZnO NWs films show a high resistance state in air ambient. Its resistance falls down on exposure to a reductive H_2S because H_2S reacts with the surface O_2^- species, which results in an enhancement of electron concentration in the ZnO NWs. (ii) In pure CoPc films, due to low coordinated structure of Co atoms in CoPc molecules, it is the most preferable sites for the chemisorptions of oxygen. H_2S can interact with CoPc films by two processes, the first one can be the direct interaction with the Co sites free from adsorbed oxygen, this process leads to very fast response and second process is the competitive displacement of the chemisorbed oxygen, which is relatively a slow process.[66] The plausible mechanism of direct interaction of H_2S with the oxygen free Co sites can be understood by the dissociation of H_2S on the metal surface under ambient condition because it is a weak acid (acid dissociation constant $pK_a = 7.05$).[67] The dissociation of H_2S results into H^+ and HS^- ions. The resulting HS^- anion mediates the reduction of CoPc (resulting in increase in the resistance) and it converts back to parent CoPc by exposing sample to the air.[68]

The second process, which is competitive displacement of the chemisorbed oxygen by H_2S from CoPc surface (responsible for response of the sensor) can be understood by the following equation:[2,36]

$$H_2S + 3O^{2-} \rightarrow H_2O + SO_2 + 6e^- \quad (10)$$

The released electrons captures the hole charge carriers of CoPc films and as a result the resistance of samples will rise on

DOI: 10.1021/acsami.5b03652
ACS Appl. Mater. Interfaces 2015, 7, 17713−17724

H_2S exposure. The recovery of the sample takes place by picking up the electron by atmospheric oxygen.

Based on these proposed mechanisms we now explain why ZnO-CoPc (25 nm) sample exhibit fast response kinetics and highest response (%) among all samples. In ZnO-CoPc (<25 nm) films, CoPc does not uniformly cover the ZnO nanowires, hence when such samples are exposed to H_2S they exhibit less response (%) and high response time due to superimposition of the response signals from CoPc (which shows the rise of resistance due to p-type conduction) and ZnO (which shows the lowering of resistance due to n-type conduction). In ZnO-CoPc (25 nm) samples, ZnO nanowires are uniformly coated with CoPc layer and exhibit very low chemisorbed oxygen therefore direct interaction of H_2S with oxygen free Co sites is preferable and hence we observe a rapid response of the ZnO-CoPc (25 nm) films. According to the morphology imaged by SEM for ZnO-CoPc (25 nm) sample the top surface of the CoPc coated ZnO NWs are interconnected with thin CoPc lamellar sheet and charge transport takes place via CoPc layer. Due to low density of holes in the CoPc layer (because of the less amount of chemisorbed oxygen) the depletion width extends more toward CoPc side from the ZnO-CoPc interface. When these heterojunction films are exposed to H_2S gas, the electrons donated by H_2S further extends the depletion region toward the CoPc layer and blocks hole conduction channel resulting in huge rise of resistance/response. The above proposed mechanism of H_2S sensing of heterojunction films is schematically shown in Figure 14. In ZnO-CoPc (50 nm) samples, the ZnO nanowires network gets covered with thick CoPc layer and hence the diffusion of H_2S inside the bulk of films results in slow response.

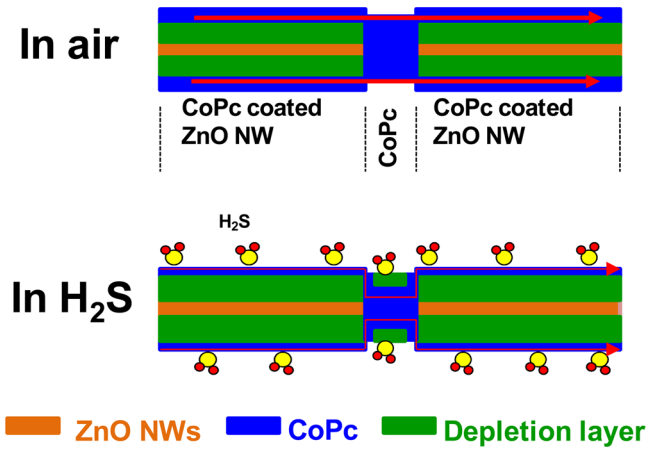

Figure 14. Schematic showing the H_2S sensing mechanism of ZnO–CoPc heterojunction films.

4. CONCLUSIONS

A cobalt phthalocyanine modified ZnO nanowires network based H_2S sensor was fabricated in two steps. First the random network of ZnO nanowires was grown on lightweight flexible BOPET sheets using hydrothermal method. In the second step these ZnO nanowires films were modified with different thickness of CoPc films. We have demonstrated that modification of n-type ZnO nanowires network by 25 nm thick p-type CoPc layer dramatically lowers the response/recovery times and improves the sensitivity for H_2S detection. The rapid response/recovery and high-sensitivity in these heterojunction films based sensor arises respectively due to direct interaction of H_2S with free Co site and blocking of conduction channel by enlargement of the depletion layer width. Our results suggest that the ZnO-CoPc heterojunction films are attractive candidate for practical H_2S sensing applications, in view of its outstanding room-temperature sensitivity, excellent dynamic properties such as rapid response/recovery and high stability.

AUTHOR INFORMATION

Corresponding Authors

*E-mail: Ajay Singh (asb_barc@yahoo.com).
*E-mail: D. K. Aswal (dkaswal@yahoo.com).

Notes

The authors declare no competing financial interest.

ACKNOWLEDGMENTS

This work was supported by the Indo-French Centre for the promotion of Advanced Research project (IFCPAR) through project 4705-C. We acknowledge the cooperative research project of the Research Institute of Electronic, Shizuoka University.

REFERENCES

(1) Pandey, S. K.; Kim, K.-H.; Tang, K.-T. A Review of Sensor-based Methods for Monitoring Hydrogen Sulfide. *TrAC, Trends Anal. Chem.* **2012**, *32*, 87–99.
(2) Aswal, D. K., Gupta, S. K., Eds.; *Sci. Technol. Chemiresistor Gas Sens.*; Nova Science Publisher: NY (USA), 2007; pp 33–94.
(3) Ramgir, N. S.; Ganapathi, S. K.; Kaur, M.; Datta, N.; Muthe, K. P.; Aswal, D. K.; Gupta, S. K.; Yakhmi, J. V. Sub-ppm H_2S Sensing at Room Temperature Using CuO Thin Films. *Sens. Actuators, B* **2010**, *151*, 90–96.
(4) Zhang, S.; Zhang, P.; Wang, Y.; Ma, Y.; Zhong, J.; Sun, X. Facile Fabrication of a Well-Ordered Porous Cu-Doped SnO_2 Thin Film for H_2S Sensing. *ACS Appl. Mater. Interfaces* **2014**, *6*, 14975–14980.
(5) Annanouch, F. E.; Haddi, Z.; Vallejos, S.; Umek, P.; Guttmann, P.; Bittencourt, C.; Llobet, E. Scalable Fabrication of High-Performance NO_2 Gas Sensors Based on Tungsten Oxide Nanowires by On-Chip Growth and RuO_2-Functionalization. *ACS Appl. Mater. Interfaces* **2015**, *7*, 6842–6851.
(6) Chen, Y.-J.; Gao, Xin-Ming.; Di, Xin-Peng.; Ouyang, Qiu-Yun.; Gao, P.; Qi, Li-Hong.; Li, Chun-Yan.; Zhu, Chun-Ling. Porous Iron Molybdate Nanorods: In situ Diffusion Synthesis and Low-Temperature H_2S Gas Sensing. *ACS Appl. Mater. Interfaces* **2013**, *5*, 3267–3274.
(7) Munz, M.; Langridge, M. T.; Devarepally, K. K.; Cox, D. C.; Patel, P.; Martin, N. A.; Vargha, G.; Stolojan, V.; White, S.; Curry, R. J. Facile Synthesis of Titania Nanowires via a Hot Filament Method and Conductometric Measurement of Their Response to Hydrogen Sulfide Gas. *ACS Appl. Mater. Interfaces* **2013**, *5*, 1197–1205.
(8) Her, Y.-C.; Yeh, B.-Y.; Huang, S.-L. Vapor–Solid Growth of p-Te/n-SnO_2 Hierarchical Heterostructures and Their Enhanced Room-Temperature Gas Sensing Properties. *ACS Appl. Mater. Interfaces* **2014**, *6*, 9150–9159.
(9) Xiao, Y.; Lu, L.; Aiqin, Z.; Zhang, Y.; Sun, L.; Huo, L.; Li, F. Highly Enhanced Acetone Sensing Performances of Porous and Single Crystalline ZnO Nanosheets: High Percentage of Exposed (100) Facets Working Together with Surface Modification with Pd Nanoparticles. *ACS Appl. Mater. Interfaces* **2012**, *4*, 3797–3804.
(10) Zang, W.; Nie, Y.; Zhu, D.; Ping, D.; Xing, L.; Xue, X. Core–Shell In_2O_3/ZnO Nanoarray Nanogenerator as a Self-Powered Active Gas Sensor with High H_2S Sensitivity and Selectivity at Room Temperature. *J. Phys. Chem. C* **2014**, *118*, 9209–9216.

DOI: 10.1021/acsami.5b03652
ACS Appl. Mater. Interfaces 2015, 7, 17713–17724

(11) Chen, J.; Wang, K.; Hartman, L.; Zhou, W. H_2S Detection by Vertically Aligned CuO Nanowire Array Sensors. *J. Phys. Chem. C* **2008**, *112*, 16017−16021.
(12) Zhang, F.; Zhu, A.; Luo, Y.; Tian, Y.; Yang, J.; Qin, Y. CuO Nanosheets for Sensitive and Selective Determination of H_2S with High Recovery Ability. *J. Phys. Chem. C* **2010**, *114*, 19214−19219.
(13) Iversen, K. J.; Spencer, M. J. S. Effect of ZnO Nanostructure Morphology on the Sensing of H_2S Gas. *J. Phys. Chem. C* **2013**, *117*, 26106−26118.
(14) Kim, J.; Yong, K. Mechanism Study of ZnO Nanorod-Bundle Sensors for H_2S Gas Sensing. *J. Phys. Chem. C* **2011**, *115*, 7218−7224.
(15) Wei, W.; Dai, Y.; Huang, B. Role of Cu Doping in SnO_2 Sensing Properties Toward H_2S. *J. Phys. Chem. C* **2011**, *115*, 18597−18602.
(16) Xue, X.; Xing, L.; Chen, Y.; Shi, S.; Wang, Y.; Wang, T. Synthesis and H_2S Sensing Properties of CuO−SnO_2 Core/Shell PN-Junction Nanorods. *J. Phys. Chem. C* **2008**, *112*, 12157−12160.
(17) Yao, K.; Caruntu, D.; Zeng, Z.; Chen, J.; Connor, C. J. O'.; Weilie, Z. Parts per Billion-Level H_2S Detection at Room Temperature Based on Self-Assembled In_2O_3 Nanoparticles. *J. Phys. Chem. C* **2009**, *113*, 14812−14817.
(18) Bai, J.; Zhou, B. Titanium Dioxide Nanomaterials for Sensor Applications. *Chem. Rev.* **2014**, *114*, 10131−10176.
(19) Kim, J.; Kim, W.; Yong, K. CuO/ZnO Heterostructured Nanorods: Photochemical Synthesis and the Mechanism of H_2S Gas Sensing. *J. Phys. Chem. C* **2012**, *116*, 15682−15691.
(20) Della Gaspera, E. D.; Guglielmi, M.; Agnoli, S.; Granozzi, G.; Post, M. L.; Bello, V.; Mattei, G.; Martucci, A. Au Nanoparticles in Nanocrystalline TiO_2-NiO Films for SPR-Based, Selective H_2S Gas Sensing. *Chem. Mater.* **2010**, *22*, 3407−3417.
(21) Liang, X.; Kim, Tae-Hyung.; Yoon, Ji-Wook.; Kwak, Chang-Hoon.; Lee, Jong-Heun. Ultrasensitive and Ultraselective Detection of H_2S using Electrospun CuO-loaded In_2O_3 Nanofiber Sensors assisted by Pulse Heating. *Sens. Actuators, B* **2015**, *209*, 934−942.
(22) Hosseini, Z. S.; Iraji Zad, A.; Mortezaali, A. Room Temperature H_2S Gas Sensor based on rather Aligned ZnO Nanorods with Flower-like Structures. *Sens. Actuators, B* **2015**, *207*, 865−871.
(23) Wang, Y.; Qu, F.; Liu, J.; Wang, Y.; Zhou, J.; Ruan, S. Enhanced H_2S Sensing Characteristics of CuO-NiO Core-Shell Microspheres Sensors. *Sens. Actuators, B* **2015**, *209*, 515−523.
(24) Hosseini, Z. S.; Mortezaali, A.; Iraji Zad, A.; Fardindoost, S. Sensitive and Selective Room Temperature H_2S Gas Sensor based on Au Sensitized Vertical ZnO Nanorods with Flower-like Structures. *J. Alloys Compd.* **2015**, *628*, 222−229.
(25) Su, P.-G.; Peng, Y.-T. Fabrication of a Room-temperature H_2S Gas Sensor based on PPy/WO_3 Nanocomposite Films by in-situ Photopolymerization. *Sens. Actuators, B* **2014**, *193*, 637−643.
(26) Ramgir, N. S.; Sharma, P. K.; Datta, N.; Kaur, M.; Debnath, A. K.; Aswal, D. K.; Gupta, S. K. Room Temperature H_2S Sensor based on Au modified ZnO Nanowires. *Sens. Actuators, B* **2013**, *186*, 718−726.
(27) Verma, M. K.; Gupta, V. A highly Sensitive SnO_2−CuO Multilayered Sensor Structure for Detection of H_2S gas. *Sens. Actuators, B* **2012**, *166−167*, 378−385.
(28) Dong, K.-Y.; Choi, J.-K.; Hwang, I.-S.; Lee, J.-W.; Kang, B. H.; Ham, D.-J.; Lee, J.-H.; Ju, B.-K. Enhanced H_2S Sensing Characteristics of Pt doped SnO_2 Nanofibers Sensors with Micro Heater. *Sens. Actuators, B* **2011**, *157*, 154−161.
(29) Balouria, V.; Kumar, A.; Samanta, S.; Singh, A.; Debnath, A. K.; Mahajan, A.; Bedi, R. K.; Aswal, D. K.; Gupta, S. K. Nano-crystalline Fe_2O_3 Thin Films for ppm level Detection of H_2S. *Sens. Actuators, B* **2013**, *181*, 471−478.
(30) Kaur, M.; Ganapathi, K.; Mukund, V.; Jain, C.; Ramgir, N. S.; Datta, N.; Bhattacharya, S.; Debnath, A. K.; Aswal, D. K.; Gupta, S. K. Selective H_2S Detection by CuO Functionalized ZnO Nanotetrapods at room temperature. *Mater. Chem. Phys.* **2014**, *143*, 1319−1324.
(31) Balouria, V.; Kumar, A.; Singh, A.; Samanta, S.; Debnath, A. K.; Mahajan, A.; Bedi, R. K.; Aswal, D. K.; Gupta, S. K.; Yakhmi, J. V. Temperature Dependent H_2S and Cl_2 Sensing Selectivity of Cr_2O_3 thin films. *Sens. Actuators, B* **2011**, *157*, 466−472.
(32) Balouria, V.; Samanta, S.; Singh, A.; Debnath, A. K.; Mahajan, A.; Bedi, R. K.; Aswal, D. K.; Gupta, S. K. Chemiresistive Gas Sensing Properties of Nanocrystalline Co_3O_4 Thin films. *Sens. Actuators, B* **2013**, *176*, 38−45.
(33) Katti, V. R.; Debnath, A. K.; Muthe, K. P.; Kaur, M.; Dua, A. K.; Gadkari, S. C.; Gupta, S. K.; Sahni, V. C. Mechanism of Drifts in H_2S sensing properties of SnO_2:CuO composite thin film sensors prepared by thermal evaporation. *Sens. Actuators, B* **2003**, *96*, 245−252.
(34) Khanna, A.; Kumar, R.; Bhatti, S. S. CuO-doped SnO_2 Thin Films as Hydrogen Sulfide Gas Sensor. *Appl. Phys. Lett.* **2003**, *82*, 4388−3.
(35) Saxena, V.; Aswal, D. K.; Kaur, M.; Koiry, S. P.; Gupta, S. K.; Yakhmi, J. V.; Kshirsagar, R. J.; Deshpande, S. K. Enhanced NO_2 Selectivity of Hybrid poly (3-hexylthiophene): ZnO-Nanowire Thin Films. *Appl. Phys. Lett.* **2007**, *90*, 043516−3.
(36) Datta, N.; Ramgir, N.; Kaur, M.; Ganapathi, S. K.; Debnath, A. K. Selective H_2S Sensing Characteristics of Hydrothermally grown ZnO-Nanowires network tailored by ultrathin CuO layers. *Sens. Actuators, B* **2012**, *166−167*, 394−401.
(37) Choi, S.-W.; Zhang, J.; Katoch, A.; Kim, S. S. H_2S Sensing Performance of Electrospun CuO-loaded SnO_2 Nanofibers. *Sens. Actuators, B* **2012**, *169*, 54−60.
(38) Saini, R.; Mahajan, A.; Bedi, R. K.; Aswal, D. K.; Debnath, A. K. Room Temperature ppb level Cl_2 Detection and Sensing Mechanism of Highly Selective and Sensitive Phthalocyanine Nanowires. *Sens. Actuators, B* **2014**, *203*, 17−24.
(39) Bohrer, F. I.; Colesniuc, C. N.; Park, J.; Ruidiaz, M. E.; Schuller, I. K.; Kummel, A. C.; Trogler, W. C. Comparative Gas Sensing in Cobalt, Nickel, Copper, Zinc, and Metal-Free Phthalocyanine Chemiresistors. *J. Am. Chem. Soc.* **2009**, *131*, 478−485.
(40) Kumar, A.; Singh, A.; Debnath, A. K.; Samanta, S.; Aswal, D. K.; Gupta, S. K.; Yakhmi, J. V. Room temperature ppb level Cl_2 Sensing using Sulphonated Copper Phthalocyanine films. *Talanta* **2010**, *82*, 1485−1489.
(41) Padma, N.; Joshi, A.; Singh, A.; Deshpande, S. K.; Aswal, D. K.; Gupta, S. K.; Yakhmi, J. V. NO_2 sensors with room temperature operation and long term stability using copper phthalocyanine thin films. *Sens. Actuators, B* **2009**, *143*, 246−252.
(42) Kumar, A.; Debnath, A. K.; Samanta, S.; Singh, A.; Prasad, R.; Veerender, P.; Singh, S.; Basu, S.; Aswal, D. K.; Gupta, S. K. Enhanced Cl_2 response of Ultrathin Bi-nuclear (cobalt−iron) Phthalocyanine films. *Sens. Actuators, B* **2012**, *171−172*, 423−430.
(43) Debnath, A. K.; Samanta, S.; Singh, A.; Aswal, D. K.; Gupta, S. K.; Yakhmi, J. V. Parts-per-billion level Chlorine Sensors with Fast Kinetics using Ultrathin Cobalt Phthalocyanine films. *Chem. Phys. Lett.* **2009**, *480*, 185−188.
(44) Singh, A.; Kumar, A.; Kumar, A.; Samanta, S.; Joshi, N.; Balouria, V.; Debnath, A. K.; Prasad, R.; Salmi, Z.; Chehimi, M. M.; Aswal, D. K.; Gupta, S. K. Bending stress Induced Improved Chemiresistive Gas Sensing Characteristics of Flexible Cobalt-Phthalocyanine Thin films. *Appl. Phys. Lett.* **2013**, *102*, 132107.
(45) Kumar, A.; Joshi, N.; Samanta, S.; Singh, A.; Debnath, A. K.; Chauhan, A. K.; Roy, M.; Prasad, R.; Roy, K.; Chehimi, M. M.; Aswal, D. K.; Gupta, S. K. Room temperature Detection of H_2S by Flexible Gold−Cobalt Phthalocyanine Heterojunction Thin films. *Sens. Actuators, B* **2015**, *206*, 653−662.
(46) Joshi, A.; Aswal, D. K.; Gupta, S. K.; Yakhmi, J. V.; Gangal, S. ZnO-Nanowires Modified Polypyrrole Films as Highly Selective and Sensitive Chlorine Sensors. *Appl. Phys. Lett.* **2009**, *94*, 103115−3.
(47) Li, M.; Meng, G.; Huang, Q.; Zhang, S. Improved Sensitivity of Polychlorinated-biphenyl-orientated Porous-ZnO surface Photovoltage Sensors from Chemisorption-formed ZnO-CuPc Composites. *Sci. Rep.* **2014**, DOI: 10.1038/srep04284.
(48) Garg, K.; Singh, A.; Majumder, C.; Nayak, S. K.; Aswal, D. K.; Gupta, S. K.; Chattopadhyay. Room Temperature Ammonia Sensor Based on Jaw like Bis-porphyrin Molecules, S. *Org. Electron.* **2013**, *14*, 1189−1196.

DOI: 10.1021/acsami.5b03652
ACS Appl. Mater. Interfaces 2015, 7, 17713−17724

(49) Yu, J.; Yu, X.; Zhang, L.; Zeng, H. Ammonia Gas Sensor Based on Pentacene Organic Field-effect Transistor. *Sens. Actuators, B* **2012**, *173*, 133−138.
(50) Park, S. H.; Kim, H. J.; Cho, M-Ho.; Yi, Y.; Cho, S. W.; Yang, J.; Kim, H. The effect of ZnO Surface Conditions on The Electronic Structure of The ZnO/CuPc Interface. *Appl. Phys. Lett.* **2011**, *98*, 082111−3.
(51) Singh, B.; Ghosh, S. Zinc oxide and Metal Phthalocyanine based Hybrid P-N Junction Diodes. *Appl. Phys. Lett.* **2013**, *103*, 133301−4.
(52) Mattioli, G.; Melis, C.; Malloci, G.; Filippone, F.; Alippi, P.; Giannozzi, P.; Mattoni, A.; Bonapasta, A. A. Zinc Oxide−Zinc Phthalocyanine Interface for Hybrid Solar Cells. *J. Phys. Chem. C* **2012**, *116*, 15439−15448.
(53) Cruickshank, A. C.; Tay, S. E. R.; Illy, B. N.; Da Campo, R.; Schumann, S.; Jones, T. S.; Heutz, S.; McLachlan, M. A.; McComb, D. W.; Riley, D. J.; Ryan, M. P. Electrodeposition of ZnO Nanostructures on Molecular Thin Films. *Chem. Mater.* **2011**, *23*, 3863−3870.
(54) Datta, N.; Ramgir, N. S.; Kumar, S.; Veerender, P.; Kaur, M.; Kailasaganapathi, S.; Debnath, A. K.; Aswal, D. K.; Gupta, S. K. Role of Various Interfaces of CuO/ZnO Random Nanowire Networks in H_2S Sensing: An Impedance and Kelvin Probe Analysis. *Sens. Actuators, B* **2014**, *202*, 1270−1280.
(55) Moulder, J. F.; Stickle, W. F.; Sobol, P. E.; Bombson, K. D. *Handbook of X-ray Photo-electron Spectroscopy*; Physical Electronics Inc.: MN, 1995.
(56) Samanta, S.; Bakas, I.; Singh, A.; Aswal, D. K.; Chehimi, M. M. In Situ Diazonium-Modified Flexible ITO-Coated PEN Substrates for the Deposition of Adherent Silver−Polypyrrole Nanocomposite Films. *Langmuir* **2014**, *30*, 9397−9406.
(57) Wang, Z. L.; Kong, X. Y.; Ding, Y.; Gao, P.; Hughes, W. L.; Yang, R.; Zhang, Y. Semiconducting and Piezoelectric Oxide Nanostructures Induced by Polar Surfaces. *Adv. Funct. Mater.* **2004**, *14*, 943−956.
(58) Samanta, S.; Aswal, D. K.; Singh, A.; Debnath, A. K.; Senthil Kumar, M.; Hayakawa, Y.; Gupta, S. K.; Yakhmi, J. V. Bias and Temperature Dependent Charge Transport in High Mobility Cobalt-Phthalocyanine Thin Films. *Appl. Phys. Lett.* **2010**, *96*, 013305.
(59) Debnath, A. K.; Samanta, S.; Singh, A.; Aswal, D. K.; Gupta, S. K.; Yakhmi, J. V.; Deshpande, S. K.; Poswal, A. K.; Surgers, C. Growth of Iron Phthalocyanine Nanoweb and Nanobrush using Molecular Beam Epitaxy. *Phys. E* **2008**, *41*, 154−163.
(60) Zhao, L.-L.; Wang, J.-Y.; Wang, X.-L.; Cheng, Z.-X.; Wang, J.; Yin, N.; Gai, Z.-G.; Jalalian, A.; Dou, Shi-Xue. Cobalt Doping Effects on Photoluminescence, Raman scattering, Crystal structure, and Magnetic and Piezoelectric Properties in ZnO Single Crystals grown from Molten Hydrous LiOH and NaOH solutions. *J. Alloys Compd.* **2015**, *628*, 303−307.
(61) Calizo, I.; Alim, A. K.; Fonoberov, V. A.; Krishnakumar, S.; Shamsa, M.; Balandinin, A. A.; Kurtz, R. Micro-Raman Spectroscopic Characterization of ZnO Quantum Dots, Nanocrystals and Nanowires. *Proc. of SPIE* **2007**, *6481*, 64810N.
(62) Markel, F.; Ferris, N. S.; Gould, I. R.; Myers, A. B. Mode-Specific Vibrational Reorganization Energies Accompanying Photo-induced Electron Transfer in the Hexamethylbenzene/Tetracyano-ethylene Charge-Transfer Complex. *J. Am. Chem. Soc.* **1992**, *114*, 6208−6219.
(63) Jennings, C.; Aroca, R.; Hor, A.-M.; Loutfy, R. O. Raman Spectra of Solid Films 3—Mg, Cu and Zn Phthalocyanine Complexes. *J. Raman Spectrosc.* **1984**, *15*, 34−37.
(64) Bartholomew, C. R.; McConnell, A. A.; Smith, W. E. Resonance Raman excitation Profile of Cobalt Phthalocyanine at Room Temperature and 10 K. *J. Raman Spectrosc.* **1989**, *20*, 595−600.
(65) Streetman, B. G.; Banerjee, S. K.; *Solid State Electronics Devices*, 6th ed.; PHI Learning Pvt. Ltd.: New Delhi, 2010.
(66) Bohrer, F. I.; Sharoni, A.; Colesniuc, C.; Park, J.; Schuller, I. K.; Kummel, A. C.; Trogler, W. C. Gas Sensing Mechanism in Chemiresistive Cobalt and Metal-Free Phthalocyanine Thin Films. *J. Am. Chem. Soc.* **2007**, *129*, 5640−5646.
(67) Qin, C.; Whitten, J. L. Interaction of S, SH and H_2S with Ag(1 0 0). *Surf. Sci.* **2005**, *588*, 83−91.
(68) Hartle, M. D.; Sommer, S. K.; Dietrich, S. R.; Pluth, M. D. Chemically Reversible Reactions of Hydrogen Sulfide with Metal Phthalocyanines. *Inorg. Chem.* **2014**, *53*, 7800−7802.

DOI: 10.1021/acsami.5b03652
ACS Appl. Mater. Interfaces 2015, 7, 17713−17724